Electronic Supplementary Material (ESM)

Polymeric micelles-based nanoagents enable phototriggering combined chemotherapy and photothermal therapy with high sensitivity

Xiaojuan Li, Weier Bao, Ming Liu, Jiaqi Meng, Zicheng Wang, Mingqi Sun, Liaoyun Zhang*, Zhiyuan Tian*

School of Chemical Sciences, University of Chinese Academy of Sciences (UCAS), Beijing 100049, China

*Correspondence author: zhangly@ucas.ac.cn (L. Zhang); zytian@ucas.ac.cn (Z. Tian)

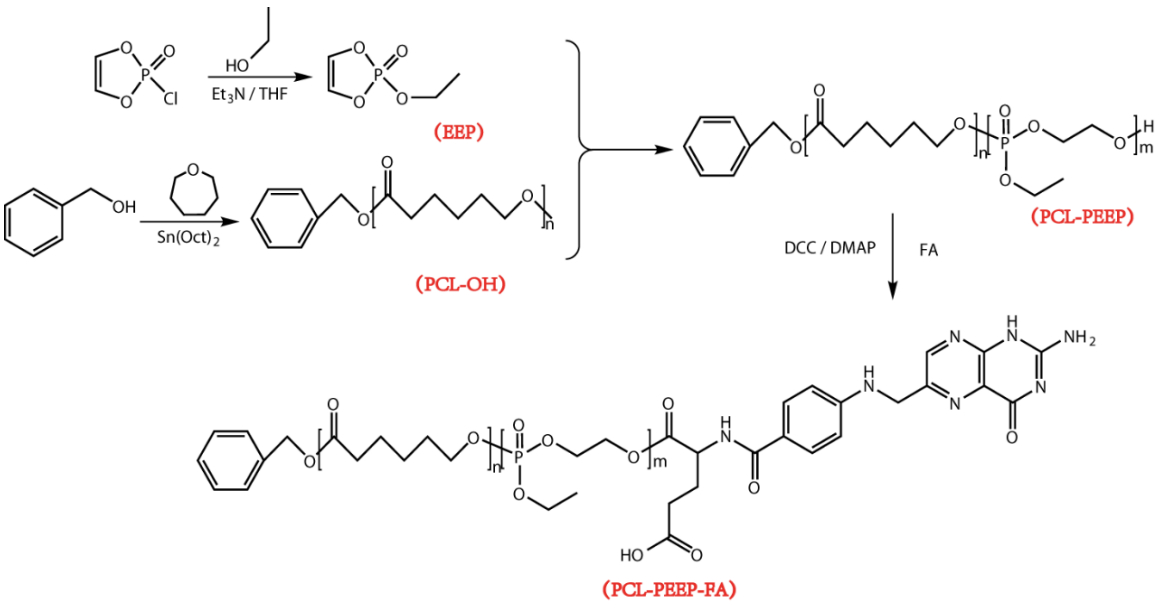

Scheme S1: Synthetic route of FA-PCL-PEEP.

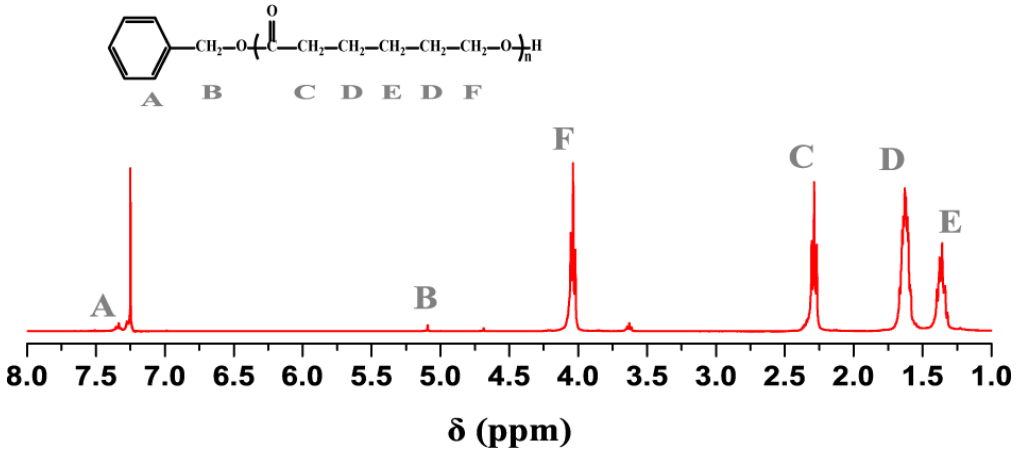

Figure S1 ^{1}H-NMR characterization result of PCL-OH. ^{1}H NMR ($CDCl_3$), δ (ppm): 7.38 (5H, ***Ar***-CH_2-), 5.11 (2H, Ar-***CH_2***-), 4.06 (2H, -C(O)-$CH_2CH_2CH_2CH_2$***CH_2***O-), 2.30 (2H, -C(O)-***CH_2***$CH_2CH_2CH_2CH_2$O-), 1.65 (2H, -C(O)-CH_2***CH_2***CH_2***CH_2***CH_2O-), 1.39 (2H, -C(O)-CH_2CH_2***CH_2***CH_2CH_2O-).

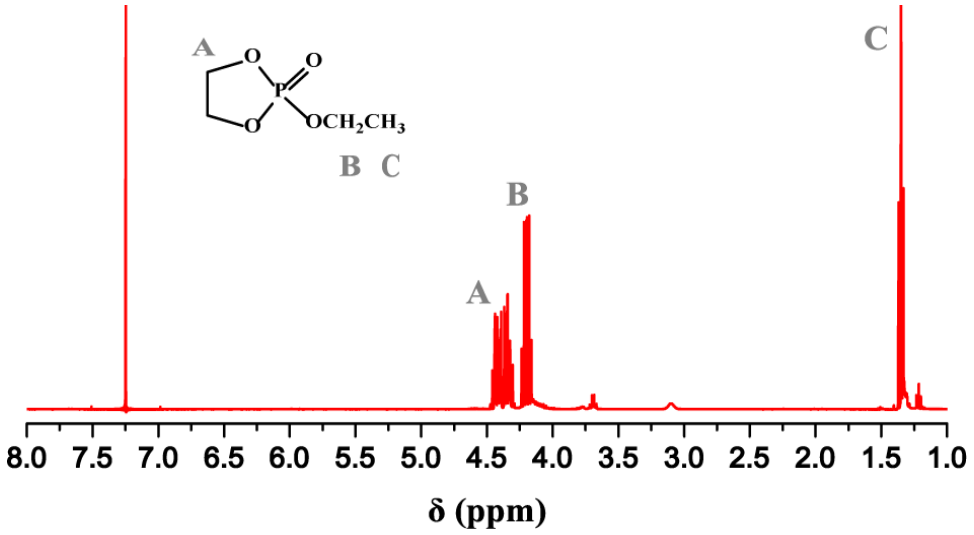

Figure S2 ^{1}H-NMR characterization result of EEP. ^{1}H NMR ($CDCl_3$), δ (ppm): 4.37 (m, O-***CH_2-CH_2***-O), 4.17 (2H, -***CH_2***CH_3), 1.34 (3H, -CH_2***CH_3***)

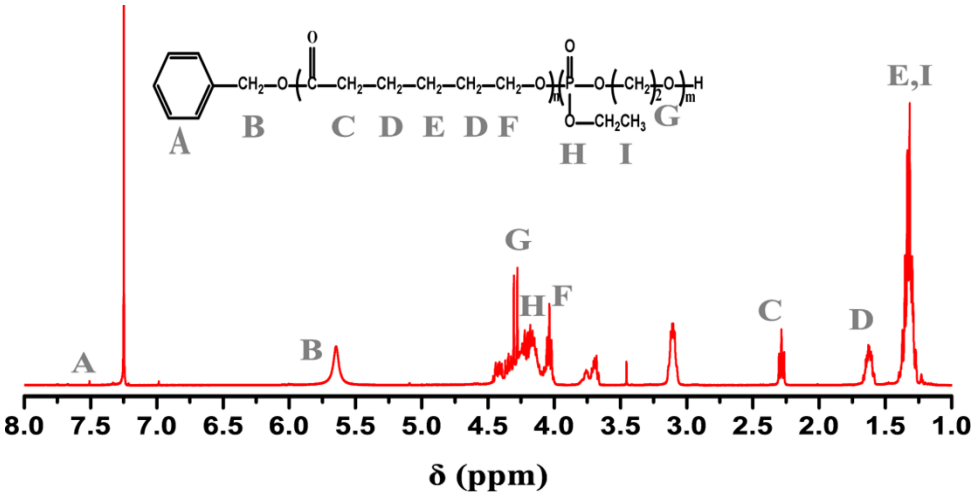

Figure S3 ^{1}H-NMR characterization result of PCL-PEEP. ^{1}H NMR ($CDCl_3$), δ (ppm): 4.29 (4H, -PO***$CH_2$$CH_2$***O-), 4.15 (2H, -O***$CH_2$***$CH_3$), 4.07 (2H, -$CH_2CH_2CH_2$***$CH_2$***OC(O)$CH_2$-), 2.32 (2H, --$CH_2CH_2CH_2CH_2$OC(O)***$CH_2$***-), 1.67 (4H, -***$CH_2$***$CH_2$***$CH_2$***$CH_2$OC(O)$CH_2$-), 1.29 (2H, -$CH_2$***$CH_2$***$CH_2CH_2$OC(O)$CH_2$- & -$OCH_2$***$CH_3$***).

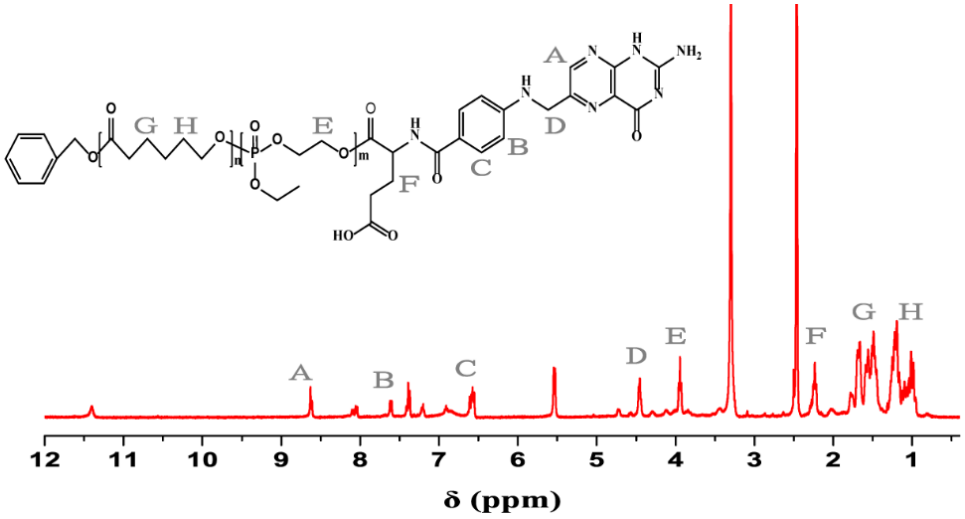

Figure S4 ^{1}H-NMR characterization result of PCL-PEEP-FA. ^{1}H NMR (DMSO), δ (ppm): 8.7 (1H, -N***CH***-C- in folate), 7.6 (2H, ***2, 6-H*** of benzene ring in folate), 6.6 (2H, ***3, 5-H*** of benzene ring in folate) 4.4 (2H, -$\boldsymbol{CH_2}$-NH- in folate), 3.8 (2H, -O-$CH_2\boldsymbol{CH_2}$-O-), 2.3 (2H, -COCH$\boldsymbol{CH_2}CH_2COOH$), 1.6 (2H, -$OCOCH_2\boldsymbol{CH_2}CH_2CH_2CH_2$-), 1.4 (2H, -$OCOCH_2CH_2CH_2\boldsymbol{CH_2}CH_2$-)

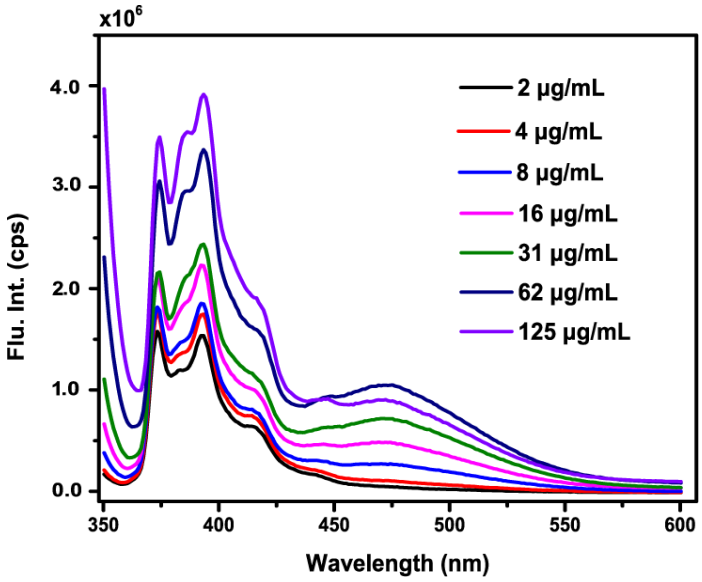

Figure S5 Fluorescence emission spectra of pyrene in PCL-PEEP aqueous solution with various concentrations.

Table S1 Photophysical properties of typical photothermal agents reported previously and T-DPPT.

Photothermal agent	Mass absorption coefficient k^{808} (L/g·cm)	Photothermal conversion efficiency η (%)	Laser power (W/cm^2)	Concentration (μg/mL)
CuS [1]	60[a]	25.7	2	100
MoS_2 [2]	28.4	24.4	1.5	50
Graphene oxide [3]	23.8	30	1.7	25
Au GNs [4]	20[a]	21	2	105
ICG [5]	26.3[a]	33	0.9	50
IR780 [6, 7]	49.46	29	4	200
Porphyrin [8, 9]	29.8	63.8	0.75	50
Polypyrrole [10]	25	51.6	2	25
T-DPPT	**80.8**	**70.1**	**0.5**	**12.5**

a) Calculated via the equation of $k = \frac{A\ (absorption)}{C\ (concentration)}$ or $k = \frac{\varepsilon\ (Molar\ extinction\ coefficient)}{M\ (Molecular\ mass)}$ based on the data in the literature.

Table S2 Formulations and antitumor performance of various chemo-PTT agents.

Formation for chemo-PTT	C (Photothermal agent) (μg/mL)	C (chemo drugs) (μg/mL)	Triggering temperature (℃)	Laser power (W/cm^2)	Cell viability (%)
ICG + DOX [11]	20	40	50	0.4 (808 nm)	24
IR780 + DOX [7]	200	10	60	4 (808 nm)	21.5
rNGO + DOX [12]	60	12	42	6 (808 nm)	36
Fe_3O_4 + DOX [13]	250	20	49	2 (808 nm)	10
CuS + DOX [1]	100	3	45	2 (980 nm)	25
Ppy + DOX [14]	10	70	47	2 (915 nm)	20
T-DPPT + PTX	**12.5**	**12.5**	**55**	**0.5 (808 nm)**	**7.9**

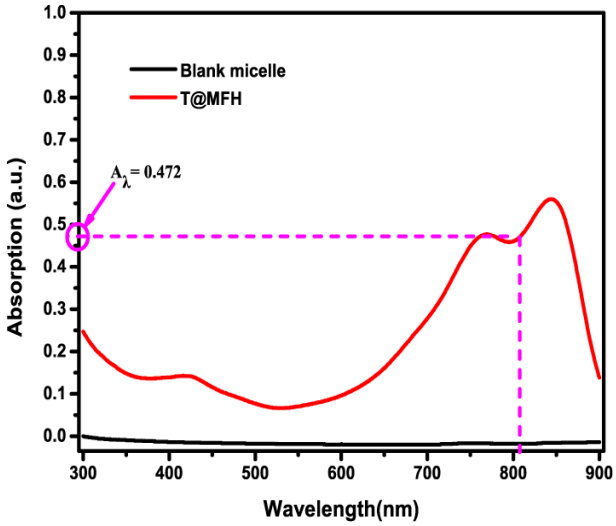

Figure S6 UV-Vis absorption spectrum of T@MFH and MFH solution presented the A_λ in Equation (1) in the main text.

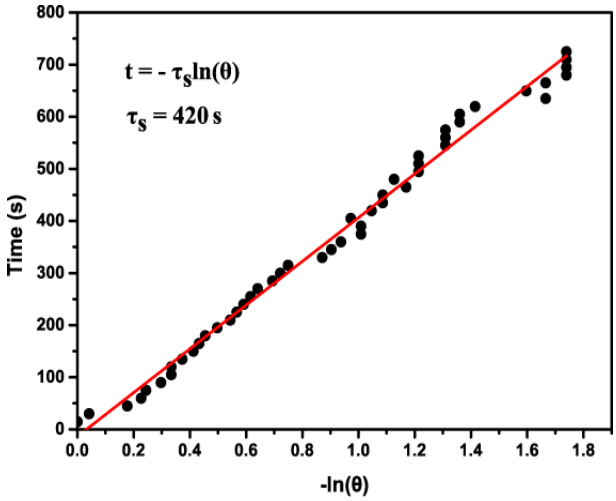

Figure S7 Photothermal profile of deionized water upon irradiation of 808-nm laser (1W/cm^2) and the subsequent cooling to room temperature for determining the time constant for heat transfer (τ) of the system discussed in the main text.

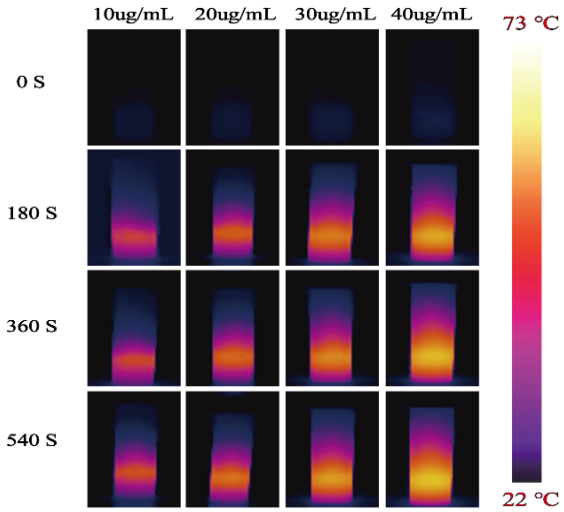

Figure S8 Infrared thermal image of T@MFH sample with various concentration upon exposing to 808-nm laser (0.5W/cm^2).

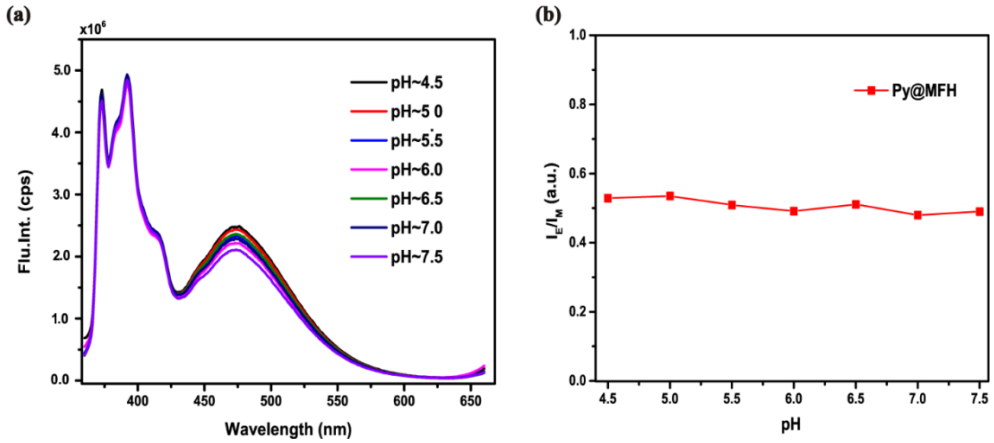

Figure S9 A range of pH fluorescence emission spectra of pyrene encapsulated-micelles in PBS after incubation in 37 ℃ water bath.

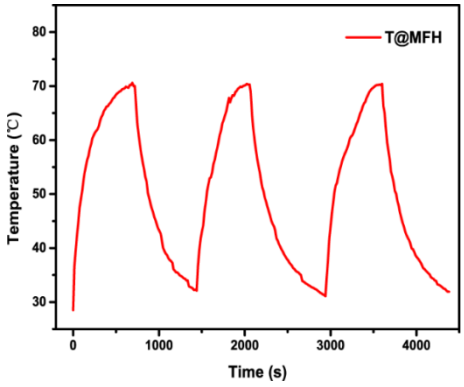

Figure S10 Photothermic stability of T@MFH upon 808 nm laser irradiation of 0.5W/cm^2 for three on/off cycles.

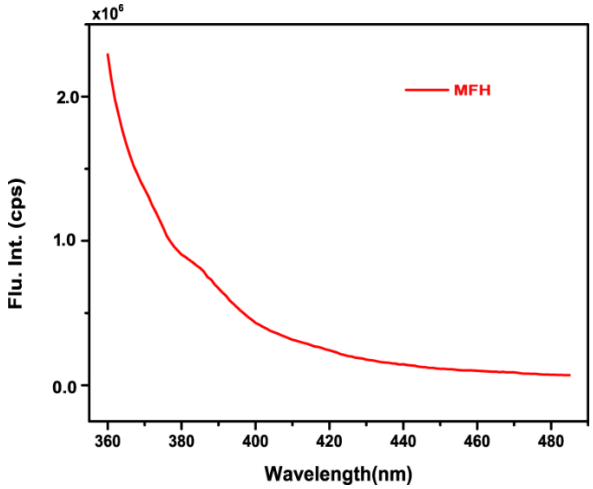

Figure S11 Fluorescence emission spectrum (Ex: 340 nm) of blank micelles (MFH).

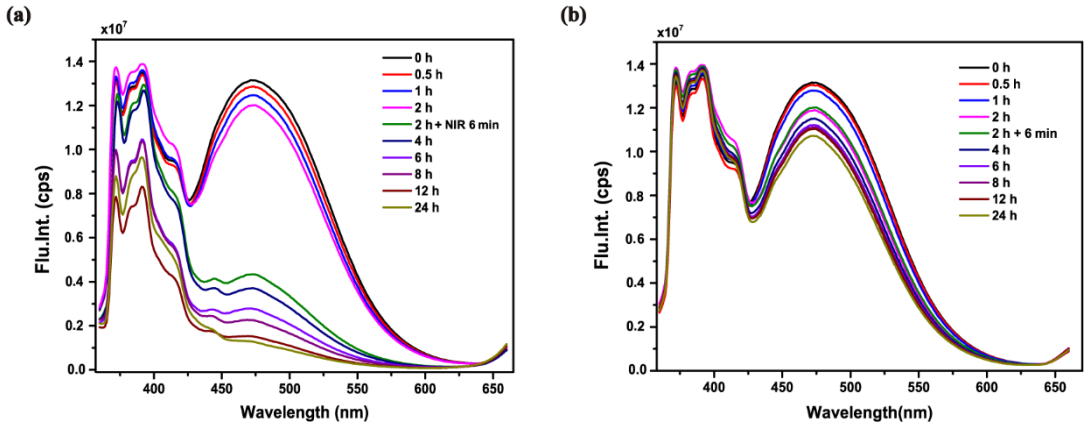

Figure S12 (a) Time-elapsed fluorescence emission spectra of T-DPPT and pyrene encapsulated-micelles in PBS after incubation in 37℃ water bath with the spectrum acquisition started when the temperature of the sample reached 37℃ and the sample exposed to 808-nm laser (0.5 W/cm^2) for 6 min 2h after the first spectrum acquisition. (b) The counterpart fluorescence emission spectra of the micelles solution without the midway 6-min irradiation of laser.

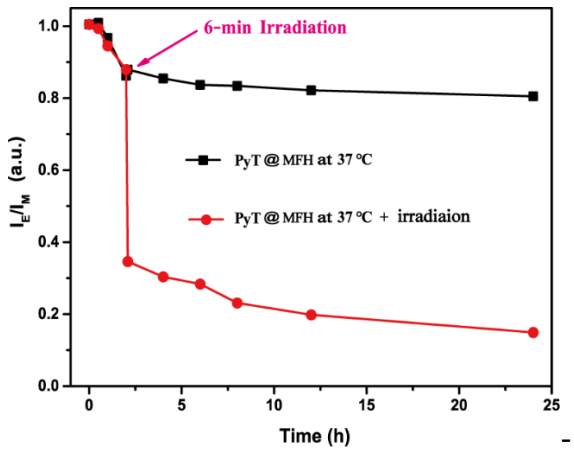

Figure S13 Plots of I_E/I_M of two parallel T-DPPT and pyrene-containing nanomicelles samples after incubation in 37℃ water bath as a function of time. Specifically, one sample was completely void of light irradiation while another underwent 6-min irradiation of 808-nm laser (0.5 W/cm^2) 2h after the starting of spectrum acquisition.

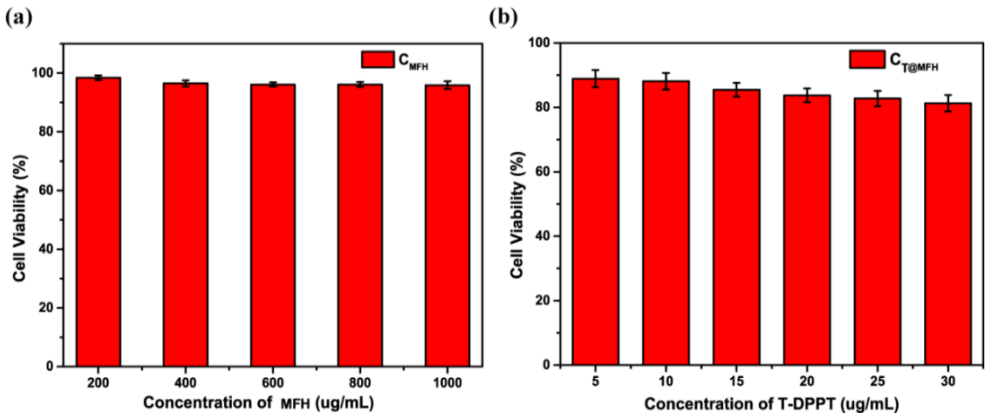

Figure S14 Cell viability of 4T1 cells after 24-h incubation with blank micelles and nanomicelles with various concentration of T-DPPT.

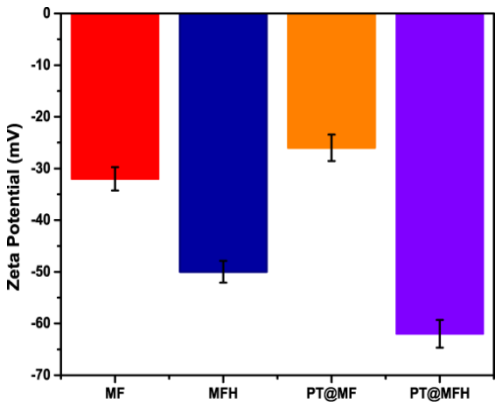

Figure S15 Surface zeta potential of HA-coated and uncoated micelles. Confirming

HA was successfully attached to the surface of micelles.

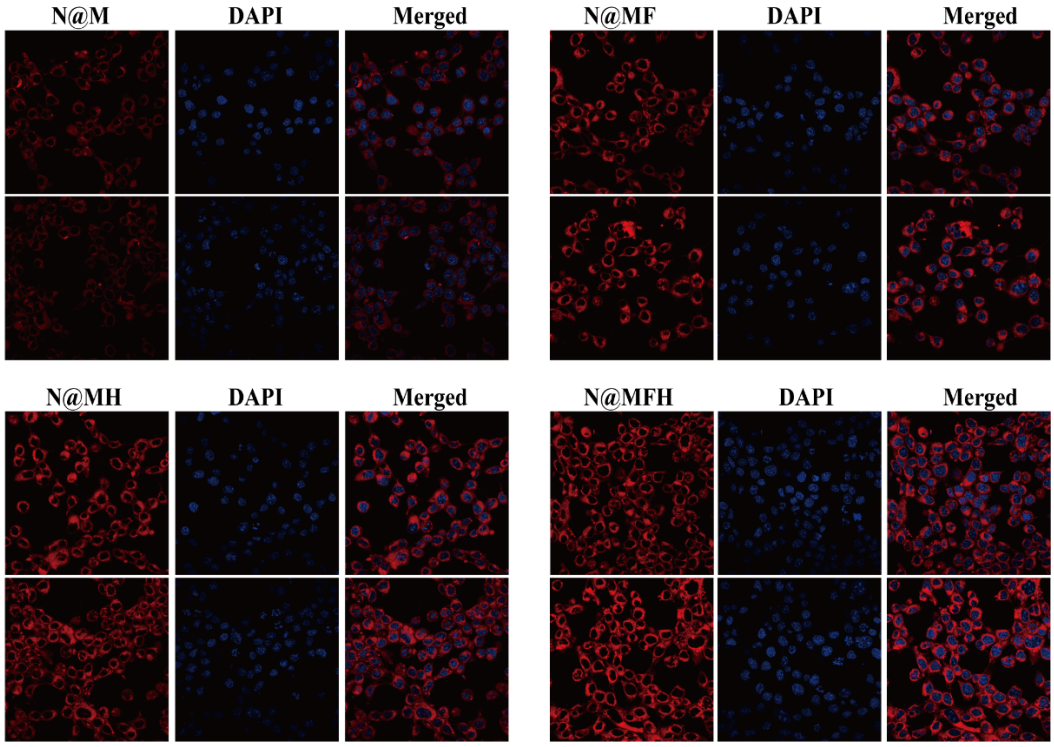

Figure S16 Two parallel sets of CLSM fluorescence imaging of 4T1 cells after treated with N@MFH + DAPI, N@MH + DAPI, N@MF + DAPI and N@M +DAPI, excited with 405nm (DAPI) and 543nm (Nile red).

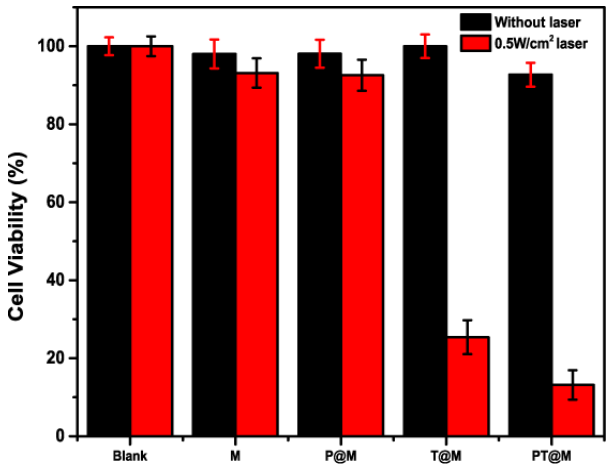

Figure S17 Cell viability of 4T1 cells after incubation with nanomicelles without functionalization of FA and HA with or without irradiation of 808-nm laser (0.5W/cm^2, 6min), respectively.

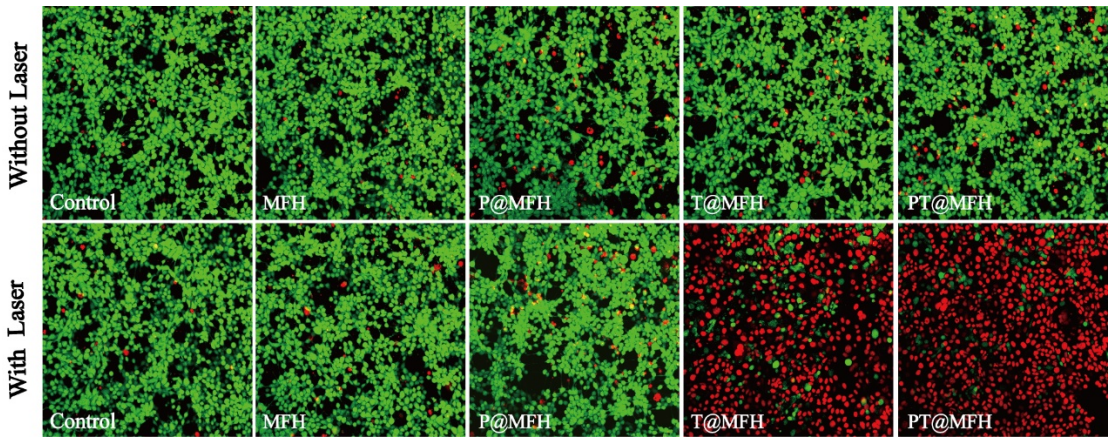

Figure S18 Fluorescence images showing the viability of 4T1 cells following different treatment. Green Calcein-AM fluorescence and red PI fluorescence indicating live and dead cells, respectively. Laser power: 0.5W/cm^2

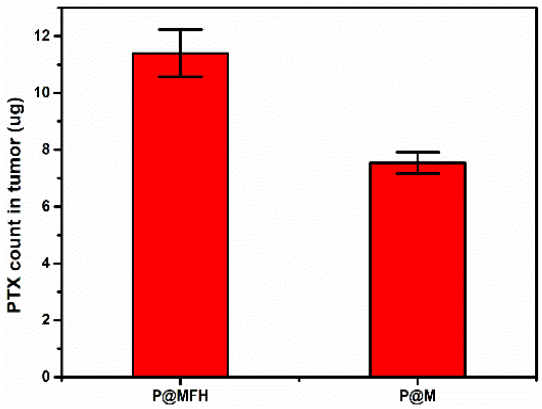

Figure S19 PTX concentration in tumor tissues acquired via HPLC method.

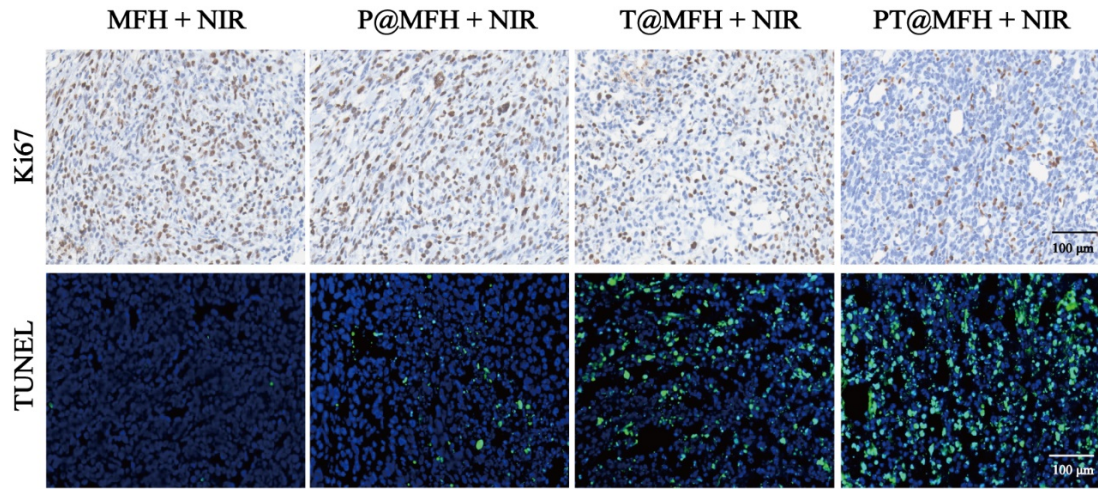

Figure S20 Fluorescence images of tumor sections with Ki67 and TUNEL staining after various treatments.

References

1. Y. Du, D. Liu, M. Sun, G. Shu, J. Qi, Y. You, Y. Xu, K. Fan, X. Xu, F. Jin, J. Wang, Q. Shen, L. Zhu, X. Ying, J. Ji, L. Wu, D. Liu and Y. Du, *Nano Research*, 2022, **15**, 2288-2299.
2. P. Li, L. Liu, Q. Lu, S. Yang, L. Yang, Y. Cheng, Y. Wang, S. Wang, Y. Song, F. Tan and N. Li, *ACS Applied Materials & Interfaces*, 2019, **11**, 5771-5781.
3. R. Lima-Sousa, D. de Melo-Diogo, C. G. Alves, E. C. Costa, P. Ferreira, R. O. Louro and I. J. Correia, *Carbohydrate Polymers*, 2018, **200**, 93-99.
4. W. Yang, H. Liang, S. Ma, D. Wang and J. Huang, *Sustainable Materials and Technologies*, 2019, **22**, e00109.
5. S. Chen, L. Zhu, Z. Du, R. Ma, T. Yan, G. Alimu, X. Zhang, N. Alifu and C. Ma, *RSC Advances*, 2021, **11**, 20850-20858.
6. C. G. Alves, R. Lima-Sousa, D. de Melo-Diogo, R. O. Louro and I. J. Correia, *International Journal of Pharmaceutics*, 2018, **542**, 164-175.
7. Y. Deng, F. Käfer, T. Chen, Q. Jin, J. Ji and S. Agarwal, *Small*, 2018, **14**, 1802420.
8. H. Mori, T. Tanaka and A. Osuka, *Journal of Materials Chemistry C*, 2013, **1**, 2500-2519.
9. B. Guo, G. Feng, P. N. Manghnani, X. Cai, J. Liu, W. Wu, S. Xu, X. Cheng, C. Teh and B. Liu, *Small*, 2016, **12**, 6243-6254.
10. K. Yang, H. Xu, L. Cheng, C. Sun, J. Wang and Z. Liu, *Advanced Materials*, 2012, **24**, 5586-5592.
11. W. Hu, X. Bai, Y. Wang, Z. Lei, H. Luo and Z. Tong, *Journal of Materials Chemistry B*, 2019, **7**, 5789-5796.
12. H. Wan, Y. Zhang, Z. Liu, G. Xu, G. Huang, Y. Ji, Z. Xiong, Q. Zhang, J. Dong, W. Zhang and H. Zou, *Nanoscale*, 2014, **6**, 8743-8753.
13. L. Wu, L. Zong, H. Ni, X. Liu, W. Wen, L. Feng, J. Cao, X. Qi, Y. Ge and S. Shen, *Biomaterials Science*, 2019, **7**, 2134-2143.
14. Z. Meng, X. Chen, Z. Liu, S. Chen, N. Yu, P. Wei, Z. Chen and M. Zhu, *RSC Advances*, 2016, **6**, 90111-90119.